



PCCP

Analysis and Visualization of Energy Densities. II. Insights from Linear-Response Time-Dependent Density Functional Theory Calculations

Journal:	<i>Physical Chemistry Chemical Physics</i>
Manuscript ID	CP-ART-08-2020-004207.R1
Article Type:	Paper
Date Submitted by the Author:	21-Oct-2020
Complete List of Authors:	<p>Pei, Zheng; Xiamen university, State Key Laboratory of Physical Chemistry of Solid Surfaces, Collaborative Innovation Center of Chemistry for Energy Materials, Fujian Provincial Key Laboratory of Theoretical and Computational Chemistry, and Department of Chemistry, Yang, Junjie; University of Oklahoma, Chemistry and Biochemistry Deng, Jingheng; University of Oklahoma, Chemistry and Biochemistry Mao, Yuezhi; Stanford University, Department of Chemistry Wu, Qin; Brookhaven National Laboratory, Center for Functional Nanomaterials Yang, Zhibo; University of Oklahoma, Chemistry and Biochemistry Wang, Bin; University of Oklahoma, Chemical, Biological and Materials Engineering Aikens, Christine; Kansas State University, Chemistry Liang, WanZhen; Xiamen university, State Key Laboratory of Physical Chemistry of Solid Surfaces, Collaborative Innovation Center of Chemistry for Energy Materials, Fujian Provincial Key Laboratory of Theoretical and Computational Chemistry, and Department of Chemistry, College of Chemistry and Chemical Engineering, Shao, Yihan; Department of Chemistry and Biochemistry, University of Oklahoma, ;</p>

Cite this: DOI: 10.1039/xxxxxxxxxx

Analysis and Visualization of Energy Densities. II. Insights from Linear-Response Time-Dependent Density Functional Theory Calculations †

Zheng Pei,^{a,#} Junjie Yang,^{b,#} Jingheng Deng,^b Yuezhi Mao,^c Qin Wu,^d Zhibo Yang,^b Bin Wang,^e Christine M. Aikens,^f Wanzhen Liang,^{*a} and Yihan Shao^{*b}

Received Date

Accepted Date

DOI: 10.1039/xxxxxxxxxx

www.rsc.org/journalname

Inspired by the analysis of Kohn-Sham energy densities by Nakai and coworkers, we extended the energy density analysis to linear-response time-dependent density functional theory (LR-TDDFT) calculations. Using ethylene-tetrafluoroethylene and oxyluciferin–water complexes as examples, distinctive distribution patterns were demonstrated for the excitation energy densities of local excitations (within a molecular fragment) and charge-transfer excitations (between molecular fragments). It also provided a simple way to compute the effective energy of both hot carriers (particle and hole) from charge-transfer excitations via an integration of the excitation energy density over the donor and acceptor grid points.

1 Introduction

Wavefunction analysis has been a central component of electronic structure calculations, dating back to the dawn of modern quantum chemistry. To characterize the charge density distribution of electronic ground state, numerous population schemes were developed to extract atomic (or fragment) charges from the one-particle density matrix, the electronic density, or the total electrostatic potential.^{1–3} These include Mulliken partitioning,⁴ Löwdin partitioning,^{5,6} atoms-in-molecule partitioning,^{7–9} natural population analysis,^{10–12} electrostatic-potential-derived charges,^{13–22} Becke-weight-based partitioning,²³ Hirshfeld partitioning,^{24–26} fragment-based Hirshfeld partitioning,²⁷ iterative Hirshfeld par-

tititioning,^{28–31} iterative Stockholder atoms partitioning,^{32,33} extended Hirshfeld partitioning,³⁴ density derived electrostatic and chemical charges,^{35–39} charge models I through V,^{1,40,41} etc. Relatedly, Fukui functions (*i.e.* atomic population changes upon electron detachment/attachment)^{42–44} were also developed to gauge the site reactivity of organic compounds.

Most of these ground-state atomic population schemes can be readily extended to excited-state calculations to analyze the excited-state electron density, as well as the corresponding attachment, detachment, and transition densities.^{45–48} Furthermore, several metrics based on the excited-state wavefunction^{45,49–58} (especially the Λ value from Peach *et al*⁵⁹ and the charge transfer number from Plasser *et al*⁴⁵) were proposed to distinguish between different types of electronic excitations (*i.e.*, local, charge transfer, and Rydberg excitations) of molecular complexes or extended molecules. Recently, the exciton (*particle-hole* pair) concept from the solid state physics perspective was also adopted by Dreuw, Plasser, and coworkers to distinguish and characterize different excitation types and extract their relevant properties.^{60–63}

During an electron excitation, the molecular system not only undergoes a charge density distribution, which is described by the detachment (hole) and attachment (particle) densities,⁶⁴ but also experiences a substantial increase in the total energy (*a.k.a.* the excitation energy). Conceptually, it is appealing to consider how the excitation energy is distributed within the molecule. Intuitively, we expect a map of the *excitation energy density* (*i.e.* a real-space distribution of the excitation energy) would show substantially increased energy density around the hole (because it requires energy to remove an electron from occupied orbitals) and possibly

^a State Key Laboratory of Physical Chemistry of Solid Surfaces, Collaborative Innovation Center of Chemistry for Energy Materials, Fujian Provincial Key Laboratory of Theoretical and Computational Chemistry, and Department of Chemistry, College of Chemistry and Chemical Engineering, Xiamen University, Xiamen 361005, P. R. China. E-mail: liangwz@xmu.edu.cn

^b Department of Chemistry and Biochemistry, University of Oklahoma, 101 Stephenson Pkwy, Norman, OK 73019, United States. E-mail: yihan.shao@ou.edu

^c Department of Chemistry, Stanford University, Stanford, CA 94305, United States.

^d Center for Functional Nanomaterials, Brookhaven National Laboratory, Upton, NY 11973, United States.

^e Center for Interfacial Reaction Engineering and School of Chemical, Biological, and Materials Engineering, Gallogly College of Engineering, University of Oklahoma, Norman, OK 73019, United States.

^f Department of Chemistry, Kansas State University, Manhattan, KS 66506, United States.

[#] These two authors contributed equally to this work.

† Electronic Supplementary Information (ESI) available: [details of any supplementary information available should be included here]. See DOI: 00.0000/00000000.

around the particle (if energy is needed to inject an electron into unoccupied orbitals there). *An integration of the excitation energy density around (well-separated) hole/particle will then yield the effective energies of both the hole and particle.* These effective energies could be quite valuable in the modeling of hole-particle pairs in photochemical processes, such as solar cells, light-emitting devices, plasmon-enhanced spectroscopy, and catalysis, etc.

In contrast to the much-developed charge density analysis, however, much less effort has been devoted to the analysis of grid-based energy distribution for electronic ground and excited states. As a matter of fact, the only work we are aware of in this direction is a grid-based energy density evaluation scheme by Nakai *et al.*, who used it to decompose the total Kohn-Sham density functional theory (KS-DFT) energy into atomic and bond energy components,^{65–67} and to analyze the MP2 and CCSD correlation energy distribution.⁶⁸ But it is rather straightforward to extend Nakai *et al.*'s grid-based energy density evaluation to the analysis of the excitation energy distribution within the linear-response time-dependent density functional (LR-TDDFT) framework.^{69–73} Such an extension will be reported below in this article.

An interesting question here is: *is the excitation energy density uniquely defined?* Needless to say, the computed LR-TDDFT excitation energy density map of a molecular system would depend on the choices of the density functional, basis set, and numerical integration grid (for solving KS-DFT and LR-TDDFT equations and for evaluating the energy density). Given a combination of functional/basis/grid, however, one component of the excitation energy density is found to be not uniquely defined within our formulation. It corresponds to the electrostatic interaction between the hole and particle (shown later in Eqs. 28 and 29), and we choose to split its contributions evenly between the hole and particle.

A second interesting question is: *is the excitation energy density an observable?* In the context of a recent perspective from Krylov on whether molecular orbitals are observables,⁴⁸ we tend to think that the excitation energy density is not a physical observable. Instead, it is only intended to be a mathematical construct for helping us assess the 3-D distribution of excitation energy.

A third question is: *given an excitation energy density, is its fragment partitioning uniquely defined?* The answer is clearly no. Multiple grid-based schemes for partitioning the electron density, such as Becke²³ and fragment-based Hirshfeld (FBH) schemes,²⁷ can be borrowed to assign the energy density at each grid point to different fragments. In addition, as pointed out by a reviewer and explained at the end of Section 2.3, the nuclear-attraction portion of the excitation energy density can also be subjected to either grid-based or nucleus-based partitioning.

This article is organized as follows. In the next section, we will briefly review Nakai *et al.*'s scheme for computing grid-based KS-DFT energy density, and then formulate our extension of this scheme for evaluating and partitioning LR-TDDFT excitation energy density. Results and discussions will be provided in Sections 3 and 4 for two model complexes (C₂H₄–C₂F₄ and OLH–H₂O). Concluding remarks will be presented in Section 5. This article complements an accompanying report, where an analysis of energy densities from a real-time time-dependent density functional

theory (RT-TDDFT) simulation⁷⁴ was presented.

2 Methods

In this work, all occupied Kohn-Sham orbitals (labeled as i and j), and virtual orbitals (labeled as a and b) are assumed to be all real. They are linear combinations of atom-centered Gaussian basis functions (labelled as μ , ν , λ , and σ),

$$\psi_i(\mathbf{r}) = \sum_{\mu} C_{\mu i} \phi_{\mu}(\mathbf{r}) \quad (1)$$

$$\psi_a(\mathbf{r}) = \sum_{\mu} C_{\mu a} \phi_{\mu}(\mathbf{r}) \quad (2)$$

with C_o and C_v collectively representing the respective molecular orbital coefficients. The ground-state one-particle density matrix is $\mathbf{P} = \mathbf{C}_o \mathbf{C}_o^{\dagger}$, namely

$$P^{\mu\nu} = \sum_i C_{\mu i} C_{\nu i} \quad (3)$$

and the corresponding electron density is

$$\rho(\mathbf{r}) = \sum_i |\psi_i(\mathbf{r})|^2 = \sum_{\mu\nu} P^{\mu\nu} \phi_{\mu}(\mathbf{r}) \phi_{\nu}(\mathbf{r}). \quad (4)$$

2.1 Grid-Based KS-DFT Ground State Energy Density

The ground-state KS-DFT energy is known to contain several components,

$$\begin{aligned} E_0 &= (E^T + E^N) + (E^J + E^K) + E^{XC} \\ &= \mathbf{P} \cdot \mathbf{h} + \frac{1}{2} \mathbf{P} \cdot \mathbf{\Pi} \cdot \mathbf{P} + \int f_{xc}(\rho(\mathbf{r})) d\mathbf{r} \end{aligned} \quad (5)$$

with the core Hamiltonian (\mathbf{h}) — kinetic (T) and nuclear attraction (N) — being

$$E^T + E^N = \sum_{\mu\nu} P^{\mu\nu} \int \phi_{\mu}(\mathbf{r}) \left[-\frac{1}{2} \nabla^2 - \sum_n \frac{Z_n}{|\mathbf{r} - \mathbf{R}_n|} \right] \phi_{\nu}(\mathbf{r}) d\mathbf{r} \quad (6)$$

where Z_n and \mathbf{R}_n are the nuclear charge and coordinates of the n -th atom, respectively. The Coulomb (J) and Hartree-Fock exchange (K) energies are,

$$E^J + E^K = \frac{1}{2} \mathbf{P} \cdot \mathbf{\Pi} \cdot \mathbf{P} = \frac{1}{2} \sum_{\mu\nu, \lambda\sigma} P^{\mu\nu} [(\mu\nu|\lambda\sigma) - \alpha_K (\mu\lambda|\nu\sigma)] P^{\lambda\sigma} \quad (7)$$

where α_K is the ratio of Hartree-Fock exchange for conventional hybrid functionals and the two-electron repulsion integrals are

$$(\mu\nu|\lambda\sigma) = \iint \phi_{\mu}(\mathbf{r}) \phi_{\nu}(\mathbf{r}) \frac{1}{|\mathbf{r} - \mathbf{r}'|} \phi_{\lambda}(\mathbf{r}') \phi_{\sigma}(\mathbf{r}') d\mathbf{r} d\mathbf{r}' \quad (8)$$

$$(\mu\lambda|\nu\sigma) = \iint \phi_{\mu}(\mathbf{r}) \phi_{\lambda}(\mathbf{r}) \frac{1}{|\mathbf{r} - \mathbf{r}'|} \phi_{\nu}(\mathbf{r}') \phi_{\sigma}(\mathbf{r}') d\mathbf{r} d\mathbf{r}' \quad (9)$$

Note that, for range-separated functionals, the Coulomb operator in Eq. 9 will be replaced with a linear combination of short-range and long-range operators.

With most quantum chemistry programs, the kinetic, nuclear attraction, Coulomb, and Hartree-Fock energy components would

be calculated analytically. But, as shown by Nakai *et al.*, like the exchange-correlation energy in Eq. 5, an energy density can also be defined for each of all other energy components,

$$\rho_0^E(\mathbf{r}) = \rho_0^T(\mathbf{r}) + \rho_0^N(\mathbf{r}) + \rho_0^J(\mathbf{r}) + \rho_0^K(\mathbf{r}) + f_{xc}(\rho(\mathbf{r})) \quad (10)$$

which together integrate into the total KS-DFT energy in Eq. 5

$$E_0 = \int \rho_0^E(\mathbf{r}) d\mathbf{r} \quad (11)$$

The kinetic energy density is well known to be,^{75,76}

$$\rho_0^T(\mathbf{r}) = \frac{1}{2} \sum_{\mu\nu} P^{\mu\nu} [\nabla\phi_\mu(\mathbf{r})] \cdot [\nabla\phi_\nu(\mathbf{r})], \quad (12)$$

whereas the nuclear attraction energy density is simply the product of the electron density and the nuclear electrostatic potential

$$\rho_0^N(\mathbf{r}) = -\rho(\mathbf{r}) \sum_n \frac{Z_n}{|\mathbf{r} - \mathbf{R}_n|}. \quad (13)$$

Once the grid value of electrostatic potential of each pair of atomic basis functions

$$V_{\lambda\sigma}(\mathbf{r}) = \int \frac{\phi_\lambda(\mathbf{r}')\phi_\sigma(\mathbf{r}')}{|\mathbf{r} - \mathbf{r}'|} d\mathbf{r}' \quad (14)$$

is pre-computed, one can readily obtain the Coulomb (J) and Hartree-Fock exchange (K) energy densities in three steps,

$$\rho_0^J(\mathbf{r}) = -\rho(\mathbf{r})V(\mathbf{r}) = \left[\sum_{\mu\nu} P^{\mu\nu} \phi_\mu(\mathbf{r})\phi_\nu(\mathbf{r}) \right] \left[\sum_{\lambda\sigma} V_{\lambda\sigma}(\mathbf{r})P^{\lambda\sigma} \right] \quad (15)$$

$$\begin{aligned} \rho_0^K(\mathbf{r}) &= -\alpha_K \sum_{\mu\nu,\lambda\sigma} \phi_\mu(\mathbf{r})\phi_\lambda(\mathbf{r})V_{\nu\sigma}(\mathbf{r})P^{\mu\nu}P^{\lambda\sigma} \\ &= -\alpha_K \sum_{\nu\sigma} \left[\sum_{\mu} P^{\mu\nu} \phi_\mu(\mathbf{r}) \right] V_{\nu\sigma}(\mathbf{r}) \left[\sum_{\lambda} P^{\lambda\sigma} \phi_\lambda(\mathbf{r}) \right] \end{aligned} \quad (16)$$

where $V(\mathbf{r}) = -\sum_{\lambda\sigma} V_{\lambda\sigma}(\mathbf{r})P^{\lambda\sigma}$ is the electrostatic potential of the total electron density. While the costs of computing $V_{\lambda\sigma}(\mathbf{r})$, $V(\mathbf{r})$, $\sum_{\mu} P^{\mu\nu} \phi_\mu(\mathbf{r})$, and $\rho_0^K(\mathbf{r})$ all scale as $O(N_{\text{bas}}^2 N_{\text{grid}})$, the most expensive term is $V_{\lambda\sigma}(\mathbf{r})$ because it takes more floating-point operations (FLOPS) to evaluate one-electron integrals than to perform matrix multiplications.

2.2 Grid-Based LR-TDDFT Excitation Energy Density

Within the LR-TDDFT framework, the (unrelaxed) difference density matrix (\mathbf{P}_ω) and transition density matrix (\mathbf{R}_ω) are defined from the transition amplitudes (\mathbf{X} and \mathbf{Y} , each of dimension $N_V \times N_o$),⁷⁷

$$\begin{aligned} \mathbf{P}_\omega &= \mathbf{P}_\omega^{\text{attach}} - \mathbf{P}_\omega^{\text{detach}} \\ &= \mathbf{C}_v(\mathbf{X}\mathbf{X}^\dagger + \mathbf{Y}\mathbf{Y}^\dagger)\mathbf{C}_v^\dagger - \mathbf{C}_o(\mathbf{X}^\dagger\mathbf{X} + \mathbf{Y}^\dagger\mathbf{Y})\mathbf{C}_o^\dagger \end{aligned} \quad (17)$$

$$\mathbf{R}_\omega = \mathbf{C}_v\mathbf{X}\mathbf{C}_o^\dagger + \mathbf{C}_o\mathbf{Y}^\dagger\mathbf{C}_v^\dagger \quad (18)$$

of each excited state. Note that \mathbf{P}_ω is a symmetric matrix, while \mathbf{R}_ω is not. Using these matrices, a compact expression for the

excitation energy is,⁷⁸

$$\omega = \mathbf{P}_\omega \cdot \mathbf{F} + \mathbf{R}_\omega \cdot (\mathbf{\Pi} + \mathbf{\Omega}) \cdot \mathbf{R}_\omega \quad (19)$$

where \mathbf{F} is the ground-state Fock matrix. Here, $\mathbf{\Omega}$ is the exchange-correlation portion of the Kohn-Sham response kernel

$$\Omega_{\mu\nu,\lambda\sigma} = \frac{\partial F_{\mu\nu}^{xc}}{\partial P^{\lambda\sigma}} = \int \left(\sum_{\xi,\xi'} \frac{\partial^2 f_{xc}}{\partial \xi \partial \xi'} \frac{\partial \xi}{\partial P^{\mu\nu}} \frac{\partial \xi'}{\partial P^{\lambda\sigma}} \right) d\mathbf{r} \quad (20)$$

with ξ and ξ' referring to alpha and beta electron densities (ρ_σ) and their gradient components (ρ_σ^x , ρ_σ^y , and ρ_σ^z). We shall call the $\mathbf{P}_\omega \cdot \mathbf{F}$ term in Eq. 19, which arises from orbital energy differences, the one-electron contribution to the excitation energy. The $\mathbf{R}_\omega \cdot (\mathbf{\Pi} + \mathbf{\Omega}) \cdot \mathbf{R}_\omega$ term, on the other hand, will be called two-electron contributions.

Similar to the ground-state KS-DFT energy, we can distribute the LR-TDDFT excitation energy in Eq. 19 over a real-space grid,

$$\omega = \int \rho^\omega(\mathbf{r}) d\mathbf{r} \quad (21)$$

with the excitation energy density components being

$$\rho^\omega(\mathbf{r}) = \rho^T(\mathbf{r}) + \rho^N(\mathbf{r}) + \rho^J(\mathbf{r}) + \rho^K(\mathbf{r}) + \rho^{XC}(\mathbf{r}). \quad (22)$$

The first two components — kinetic and nuclear attraction energy densities — come only from the one-electron term ($\mathbf{P}_\omega \cdot \mathbf{F}$)

$$\rho^T(\mathbf{r}) = \frac{1}{2} \sum_{\mu,\nu,i} P_{\omega}^{\mu\nu} [\nabla\phi_\mu(\mathbf{r})] \cdot [\nabla\phi_\nu(\mathbf{r})] \quad (23)$$

$$\rho^N(\mathbf{r}) = -\rho_{\text{diff}}(\mathbf{r}) \sum_n \frac{Z_n}{|\mathbf{r} - \mathbf{R}_n|} \quad (24)$$

where the (unrelaxed) difference density is

$$\rho_{\text{diff}}(\mathbf{r}) = \sum_{\mu\nu} P_{\omega}^{\mu\nu} \phi_\mu(\mathbf{r})\phi_\nu(\mathbf{r}) \quad (25)$$

The last three components (Coulomb, Hartree-Fock exchange, and exchange-correlation) of the excitation energy density in Eq. 22, on the other hand, all include both one-electron contributions (associated with difference density matrix) and two-electron contributions (associated with transition density matrix). Amongst, the Coulomb (J) and Hartree-Fock exchange (K) components can be evaluated as,

$$\rho^J(\mathbf{r}) = \sum_{\mu\nu,\lambda\sigma} \phi_\mu(\mathbf{r})\phi_\nu(\mathbf{r})V_{\lambda\sigma}(\mathbf{r}) \left(P_{\omega}^{\mu\nu} P^{\lambda\sigma} + R_{\omega}^{\mu\nu} R_{\omega}^{\lambda\sigma} \right) \quad (26)$$

$$\rho^K(\mathbf{r}) = -\alpha_K \sum_{\mu\nu,\lambda\sigma} \phi_\mu(\mathbf{r})\phi_\lambda(\mathbf{r})V_{\nu\sigma}(\mathbf{r}) \left(P_{\omega}^{\mu\nu} P^{\lambda\sigma} + R_{\omega}^{\mu\nu} R_{\omega}^{\lambda\sigma} \right) \quad (27)$$

The computation of $\rho^J(\mathbf{r})$ and $\rho^K(\mathbf{r})$ can follow a similar procedure as that of ground-state energy components shown in Eqs. 15 and 16, but it will involve more matrix multiplications. A subtle but important issue here is that the two-electron contribution to $\rho^K(\mathbf{r})$ in Eq. 27, is not uniquely defined. This can be easily understood within the MO representation, where this excitation energy density

component becomes

$$\begin{aligned} \rho_2^K(\mathbf{r}) &= -\alpha_K \sum_{\mu\nu,\lambda\sigma} \phi_\mu(\mathbf{r})\phi_\lambda(\mathbf{r})V_{\nu\sigma}(\mathbf{r})R_\omega^{\mu\nu}R_\omega^{\lambda\sigma} \\ &= -\alpha_K \sum_{ia,jb} [\psi_a(\mathbf{r})\psi_b(\mathbf{r})V_{ij}(\mathbf{r})X_{ai}X_{bj} + \psi_a(\mathbf{r})\psi_j(\mathbf{r})V_{bi}(\mathbf{r})X_{ai}Y_{bj} \\ &\quad + \psi_b(\mathbf{r})\psi_i(\mathbf{r})V_{aj}(\mathbf{r})Y_{ai}X_{bj} + \psi_i(\mathbf{r})\psi_j(\mathbf{r})V_{ab}(\mathbf{r})Y_{ai}Y_{bj}] \quad (28) \end{aligned}$$

and the first term (associated with $\mathbf{X} \otimes \mathbf{X}$) would dominate. For charge-transfer excitations, this density would be concentrated mainly on the electron acceptor, where virtual orbitals a and b reside. On the other hand, an equivalent way for distributing the two-electron Hartree-Fock exchange energy (that integrates to the same total exchange energy contribution to the excitation energy) is to transpose both (nonsymmetric) transition density matrices in Eq. 27,

$$\begin{aligned} \rho_2^K(\mathbf{r}) &= -\alpha_K \sum_{\mu\nu,\lambda\sigma} \phi_\mu(\mathbf{r})\phi_\lambda(\mathbf{r})V_{\nu\sigma}(\mathbf{r})R_\omega^{\nu\mu}R_\omega^{\sigma\lambda} \\ &= -\alpha_K \sum_{ia,jb} [\psi_i(\mathbf{r})\psi_j(\mathbf{r})V_{ab}(\mathbf{r})X_{ai}X_{bj} + \psi_b(\mathbf{r})\psi_i(\mathbf{r})V_{aj}(\mathbf{r})X_{ai}Y_{bj} \\ &\quad + \psi_a(\mathbf{r})\psi_j(\mathbf{r})V_{bi}(\mathbf{r})Y_{ai}X_{ai} + \psi_a(\mathbf{r})\psi_b(\mathbf{r})V_{ij}(\mathbf{r})Y_{ai}Y_{bj}] \quad (29) \end{aligned}$$

For charge-transfer excitations, this produces an energy density mostly on the donor moiety, where occupied orbitals i and j are located. In this work, we will use the average between these two distributions (Eqs. 28 and 29). For charge-transfer excitations, this means that the two-electron Hartree-Fock exchange energy (*i.e.* the electrostatic interaction between the particle and the hole) is evenly split between the donor and acceptor moieties.

Finally, the one-electron and two-electron contributions to the exchange-correlation term in Eq. 22 are

$$\rho_1^{XC}(\mathbf{r}) = \sum_{\mu\nu} \left(\sum_{\xi} \frac{\partial f_{xc}}{\partial \xi} \frac{\partial \xi}{\partial P^{\mu\nu}} \right) P_\omega^{\mu\nu} \quad (30)$$

$$\rho_2^{XC}(\mathbf{r}) = \sum_{\mu\nu,\lambda\sigma} R_\omega^{\mu\nu} \left(\sum_{\xi,\xi'} \frac{\partial^2 f_{xc}}{\partial \xi \partial \xi'} \frac{\partial \xi}{\partial P^{\mu\nu}} \frac{\partial \xi'}{\partial P^{\lambda\sigma}} \right) R_\omega^{\lambda\sigma} \quad (31)$$

2.3 Real-Space Partitioning Schemes

Two sets of weights for real-space grid points — Becke weights²³ and those from Fragment-Based Hirshfeld (FBH) analysis²⁷ — will be employed to partition the charge and energy densities onto different fragments.

Within the Becke scheme, which is widely employed for integrating the exchange-correlation contributions to the KS-DFT energy and Fock matrix, Lebedev quadrature points are added around each atom. The weight of each grid point is defined as

$$w_n(\mathbf{r}) = \frac{P_n(\mathbf{r})}{\sum_{m \in \text{atoms}} P_m(\mathbf{r})} \quad (32)$$

with $P_m(\mathbf{r})$ being polynomial functions of the distance between the grid point from the m -th nucleus. For each molecular fragment

(A), the collective weight is

$$w_A^{\text{Becke}}(\mathbf{r}) = \sum_{n \in A} w_n(\mathbf{r}). \quad (33)$$

Within the FBH analysis, one first computes the electron densities for isolated fragments, $\rho_B^{\text{isolated}}(\mathbf{r})$. The “promolecule” density for a molecular complex is defined as a sum of these fragment densities,

$$\rho^{\text{promolecule}}(\mathbf{r}) = \sum_B \rho_B^{\text{isolated}}(\mathbf{r}) \quad (34)$$

For each real-space grid point, a weight, $w_A(\mathbf{r})$, can be assigned to each fragment

$$w_A^{\text{FBH}}(\mathbf{r}) = \frac{\rho_A^{\text{isolated}}(\mathbf{r})}{\rho^{\text{promolecule}}(\mathbf{r})} \quad (35)$$

Note that FBH population was used previously to construct constrained density functional theory (CDFT) states of molecular complexes.^{27,79,80}

Using either set of atomic weights, we can partition the difference electron density in Eq. 25 and the excitation energy density in Eq. 22 onto different fragments,

$$(\Delta Q)_A = \int w_A(\mathbf{r})\rho_{\text{diff}}(\mathbf{r}) d\mathbf{r} \quad (36)$$

$$\omega_A = \int w_A(\mathbf{r})\rho^\omega(\mathbf{r}) d\mathbf{r} \quad (37)$$

In this work, the fragment charge in Eq. 36 was computed using the relaxed difference densities.

In these partition schemes, the energy density components are all assigned to the fragments using the weight functions in Eqs. 32 and 35. For the nuclear attraction portion of the excitation energy density in Eq. 24, for instance, the fragment values are

$$\omega_A^{N,g} = \int w_A(\mathbf{r})\rho^N(\mathbf{r}) d\mathbf{r} = - \int w_A(\mathbf{r})\rho_{\text{diff}}(\mathbf{r}) \sum_n \frac{Z_n}{|\mathbf{r} - \mathbf{R}_n|} d\mathbf{r} \quad (38)$$

which amounts to a grid-based fragment partitioning of the unrelaxed difference density in Eq. 25. A reviewer drew our attention to an alternative nucleus-based partitioning,

$$\omega_A^{N,n} = - \int \rho_{\text{diff}}(\mathbf{r}) \sum_{n \in A} \frac{Z_n}{|\mathbf{r} - \mathbf{R}_n|} d\mathbf{r}. \quad (39)$$

The average of the grid-based and nucleus-based partitioning was adopted by Nakai and coworkers in the ground state energy density analysis (see Eq. 26 in Ref. 66). This hybrid partitioning scheme worked well in the decomposition of the instantaneous RT-TDDFT energy in the accompanying paper.⁷⁴

We also tried both schemes to partition the nuclear attraction contribution to the excitation energy density of the $\text{C}_2\text{H}_4\text{-C}_2\text{F}_4\text{-F}$ configuration. For charge-transfer excitations, as shown in Table S12, the nucleus-based partitioning yielded rather different values (by over 150 eV) for the fragment nuclear-attraction energies. As a result, neither it nor a hybrid scheme can adequately cancel one-electron Coulomb and other contributions to the fragment excitation energy. Therefore, only the grid-based partitioning in

Eq. 38 will be utilized in our analysis below in the Results section.

2.4 Characterization of Electronic Excitations

In our work, besides fragment charges, two other metrics will be used to distinguish charge-transfer excitations from local excitations. The first one is the widely-used Λ factor proposed by Peach *et al.*⁵⁹ For a given LR-TDDFT excited state, it will be computed as

$$\Lambda = \frac{\sum_{a,i} O_{ai} |X_{ai} + Y_{ai}|^2}{\sum_{a,i} |X_{ai} + Y_{ai}|^2} \quad (40)$$

where O_{ai} is the overlap of the moduli of the a -th virtual orbital and the i -th occupied orbital,

$$O_{ai} = \int |\psi_a(\mathbf{r})| |\psi_i(\mathbf{r})| d\mathbf{r}. \quad (41)$$

Alternatively, one can utilize the detachment (“hole”) and attachment (“particle”) densities, which can be computed by plugging the corresponding unrelaxed difference density matrix components in Eq. 17 into Eq. 25. In a recent work, the overlap of detachment (or attachment) densities from separate LR-TDDFT calculations was employed to compare excited states computed using different basis sets.⁸¹ In this work, the overlap between the attachment and detachment densities of each excited state proposed first by Etienne^{51,52}

$$S_{DA} = \int [\rho^{\text{detach}}(\mathbf{r})]^{\frac{1}{2}} [\rho^{\text{attach}}(\mathbf{r})]^{\frac{1}{2}} d\mathbf{r} \quad (42)$$

will be used as an alternative metric for assessing its character.

For each excited state, both criteria will fall in the range of [0,1], with a smaller value indicating a stronger charge-transfer character.

3 Computational Details

Two model complexes were used to demonstrate the distribution of the excitation energy densities. The first was the ethylene-tetrafluoroethylene ($C_2H_4-C_2F_4$) complex, which was widely used in the development of the range-separated functionals.^{82,83} Both C_2H_4 and C_2F_4 were optimized using the ω B97X-D functional⁸⁴ and 6-311++G(d,p) basis set.⁸⁵ Then, these monomers were combined together (without further geometry relaxation) into three different configurations:

- Cofacial (labeled as **F**, Figure 1). Two monomers were stacked on top of each other with a 5 Å distance in between.
- Planar 1 (labeled as **P1**, Figure 2). Two monomers laid side-by-side with a 5 Å distance between the closest carbon atoms.
- Planar 2 (labeled as **P2**, Figure 3). Two monomers laid end-to-end with a 5 Å distance between the closest carbon atoms.

The second was the oxyluciferin molecule (OLH or OxyLH₂), where 6'-oxygen is protonated, in complex with a water molecule. Its anionic form has been shown to be the light emitter in firefly bioluminescence.⁸⁶ Three different types of configurations would also be studied:

- Hydrogen-bonded 1 and 2 (labelled as **HB1** and **HB2**, Figure 5). Water molecule formed a hydrogen bond with the 5'-oxygen or 6'-oxygen of OLH. Both complexes were optimized at ω B97X-D/6-311++G(d,p) level of theory.
- T-shape (labelled as **T**, Figure 6). Water molecule formed a T-shape complex with OLH, with its one O-H bond pointing towards the center of the benzene ring of OLH. A series of geometries were obtained via restrained geometry optimization with varying distances (1.6, 1.7, 1.8, 1.9, 2.0, and 2.1 Å) between the water hydrogen atom and the center of the OLH benzene ring.

The evaluation and partitioning of excitation energy densities were implemented within a development version of the PYSCF software package.⁸⁷ Standard and restrained geometry optimization and LR-TDDFT/TIP3P excitation energy calculations of different OLH-H₂O configurations were carried out by the Q-CHEM software package.⁸⁸ All geometries used in this article, together with their ω B97X-D/6-311++G(d,p) energies as computed by Q-CHEM, are provided in the Electronic Supplementary Information.

4 Results

4.1 Ground-State Energy Density

Before proceeding to present our results on the excitation energy density of the two molecular complexes, it would be beneficial to analyze and understand the ground-state energy densities. This has already been carried out in the accompanying paper, where the ground-state energy densities of N₂ molecule and a small Ag₄ cluster were analyzed. Here is a summary of our key understandings of the ground-state energy densities:

- The kinetic energy density (ρ_0^T) and the Coulomb energy density (ρ_0^J) are always positive. In contrast, the nuclear attraction energy density (ρ_0^N), Hartree-Fock exchange energy density (ρ_0^K), and exchange-correlation energy density (ρ_0^{XC}) are all negative. ρ_0^K and ρ_0^{XC} are substantially smaller in the magnitude than other energy densities.
- The total ground-state energy density (ρ_0^E) is usually negative, and thus has an opposite sign as the charge density. But ρ_0^E has a positive value in a “donut” region around each nucleus, due to a slower decay of the kinetic energy density there.
- All energy density components decay rapidly away from the molecule.

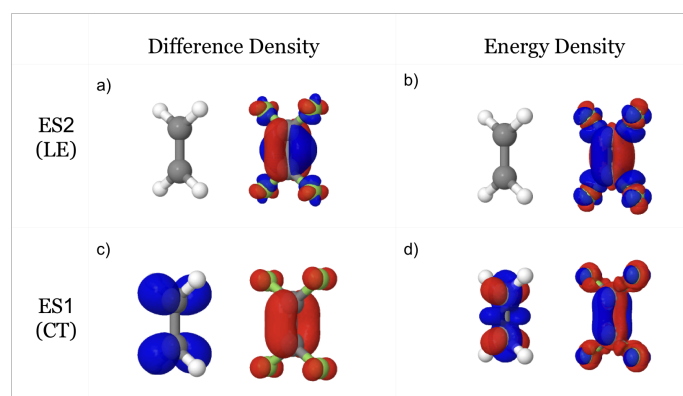
4.2 Ethylene-Tetrafluoroethylene ($C_2H_4-C_2F_4$) Complexes

Ethylene-tetrafluoroethylene is an interesting system. With the HOMO of the complex coming from C_2F_4 and the LUMO from C_2H_4 , one of the low-lying excited states involves a charge transfer between these orbitals from different fragments. Such a charge-transfer state can have a lower energy than local excitations on either C_2F_4 or C_2H_4 fragment, especially with the use of conventional hybrid density functionals and smaller basis sets.

Table 1 collects information on the lowest two excitations for each of the three $C_2H_4-C_2F_4$ configurations, which were obtained

Table 1 Excitation character metrics (Λ and S_{DA}), FBH fragment charges (ΔQ_A), FBH fragment excitation energies (ω_A) for the lowest local excitation and charge-transfer excitations of three $C_2H_4-C_2F_4$ configurations. Obtained from LR-TDDFT calculations using the PBE0 functional and 6-31G(d) basis set.

Configuration	ES#	Λ	S_{DA}	Q_A (a.u.)		ω_A or ω (eV)		
				C_2H_4	C_2F_4	C_2H_4	C_2F_4	Total
F	2	0.623	0.631	0.000	0.000	-0.003	7.129	7.125
P1	1	0.611	0.628	-0.010	0.010	0.026	7.074	7.099
P2	1	0.623	0.631	-0.001	0.001	0.005	7.121	7.126
F	1	0.092	0.042	-0.997	0.997	0.315	6.698	7.012
P1	2	0.015	0.006	-0.990	0.990	0.426	6.819	7.244
P2	2	0.005	0.003	-0.999	0.999	0.466	6.835	7.301

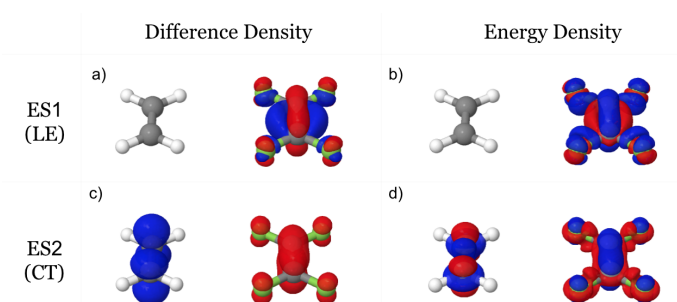
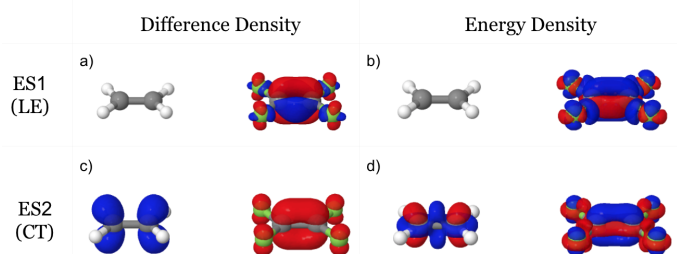
**Fig. 1** Difference density and excitation energy density plots (isovalue = 0.01 au; red = negative) for the lowest (a, b) local excitation and (c, d) charge transfer excitation of the **F** (stacked) configuration of the $C_2H_4-C_2F_4$ complex from LR-TDDFT calculations with PBE0 functional and 6-31G(d) basis set.

from LR-TDDFT calculations using the PBE0 functional⁸⁹ and 6-31G(d) basis set.^{90,91} The corresponding difference densities and excitation energy densities are shown in Figures 1, 2, and 3.

The charge-transfer character of each excited state can be first assessed by examining the FBH fragment charges as defined in Eq. 36. For the cofacial configuration (**F**), our LR-TDDFT/PBE0/6-31G(d) calculation predicted a charge-transfer excited state (with $0.997 e^-$ within the FBH scheme shifted from C_2F_4 to C_2H_4 ; see Figure 1c for the density change) to be lower than a local excitation on C_2F_4 (with $0.000 e^-$ shifted; Figure 1a). On the other hand, for two other configurations (**P1** and **P2**), the charge-transfer state (with 0.990 or $0.999 e^-$; Figures 2c and 3c) has a higher energy than the corresponding local excitations. Similar amounts of charge transfer between the fragments can be found in Table S10 for the Becke and ESP-derived charge schemes.

Two other metrics for characterizing excited states behaved very similarly. In Table 1, Λ and S_{DA} values were shown to be consistently smaller than 0.1 for charge-transfer states, and their values fell in the range of 0.60–0.65 for locally excited states. This confirms that the S_{DA} value can also be useful for distinguishing charge-transfer excitations from local excitations.

As expected, the excitation energy densities were shown in Figures 1, 2, and 3 to be concentrated on a molecular fragment

**Fig. 2** Difference density and excitation energy density plots (isovalue = 0.01 au; red = negative) for the lowest (a, b) local excitation and (c, d) charge transfer excitation of the **P1** (planar side-by-side) configuration of the $C_2H_4-C_2F_4$ complex from LR-TDDFT calculations with PBE0 functional and 6-31G(d) basis set.**Fig. 3** Difference density and excitation energy density plots (isovalue surface of 0.01 au; red = negative) for the lowest (a, b) local excitation and (c, d) charge transfer excitation of the **P2** (planar end-to-end) configuration of the $C_2H_4-C_2F_4$ complex from LR-TDDFT calculations with PBE0 functional and 6-31G(d) basis set.

for localized excitations, and distributed over both fragments for charge-transfer excitations. We can easily recognize two distinct contributions to each excitation energy density:

- “normal” contribution, which has the opposite sign (color) as the difference density. (The corresponding natural transition orbitals⁹² of these lowest CT states are shown in Fig. S1 of SI). This is similar to our observation for the ground state energy density as summarized above in Section 4.1. For the lowest charge-transfer excitation of the cofacial configuration, for example, an electron was detached from C_2F_4 HOMO (see the red “cloud” in Figure 1c). Accordingly, one can recognize

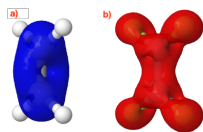


Fig. 4 Kinetic energy density (isovalue = 0.01 au) for a) C_2H_4 LUMO and b) C_2F_4 HOMO. The latter was multiplied by -1 to be consistent with its contribution to the kinetic energy density of the charge-transfer excitation.

a positive (blue) energy density of a similar shape on C_2F_4 in Figure 1d.

- kinetic energy contribution, which has the same sign (color) as the different density but has a very different shape. For the cofacial configuration, the kinetic energy densities are shown in Fig. 4 for C_2H_4 LUMO and C_2F_4 HOMO, which combine together to yield the kinetic energy density of the lowest charge-transfer excitation. Such a contribution is clearly responsible for the extra features within and near the molecular planes in the excitation energy density plots in, for instance, Figure 1d.

When the excitation energy densities are integrated over each fragment according to Eq. 37, the total excitation energy is divided into fragment contributions. In accordance with our expectation, the excitation energy was shown in Table 1 to concentrate on one fragment (C_2F_4 in tested cases) for local excitations. For the lowest charge-transfer excitation of each configuration, significant (>0.3 eV) and positive excitation energy values were observed on both donor and acceptor fragments. However, the value on the donor fragment (C_2F_4 in these cases) are substantially larger, reflecting that (the absolute value of) HOMO energy (*i.e.* ionization potential within Koopman's theorem) is usually larger than the LUMO energy (*i.e.* electron affinity within Koopman's theorem). For instance, the electron donors contributed 6.7–6.8 eV to the total excitation energies while only 0.3–0.5 eV came from electron acceptors (see Table 1).

For higher charge-transfer excitation states, the electrons can be excited into LUMO+1 or higher unoccupied orbitals. In those cases, the acceptor portion of the excitation energy can become larger. The C_2H_4 fragment, for instance, serves as an electron acceptor of the fourth charge-transfer excited state from a TDDFT-PBE/6-31G(d) calculation (see Table S1), and contributed 2.665 eV to the excitation energy out of a total of 8.078 eV. For those states, natural transition orbitals⁹² should be used to analyze the difference densities and the corresponding kinetic energy contribution to the excitation energy density. As we mentioned in the introduction, the fragment excitation energies on the donor (acceptor) fragment can be regarded as effective energies of the “hole” (“particle”) in the charge-transfer excitations.

4.3 Oxyluciferin–Water Complexes

The neutral oxyluciferin molecule (OLH) can form multiple hydrogen bond complexes with a single water molecule. As shown in Figure 5, both 5'-oxygen (on the thiazole ring) and 6'-oxygen (on the benzothiazole ring) could serve as the hydrogen bond acceptor, leading to two complexes (**HB1** and **HB2**). As indicated by the

BSSE-corrected binding energies in Table 2, these hydrogen bonds could stabilize the complex by 4.0 to 6.5 kcal/mol.

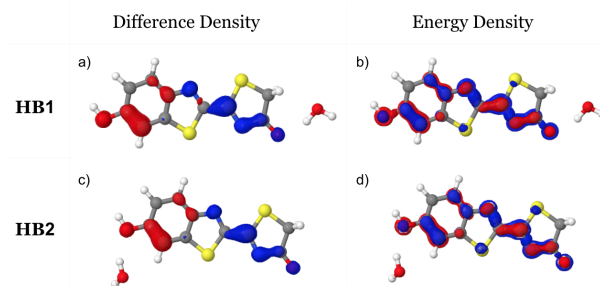


Fig. 5 Difference density and excitation energy density plots (isovalue = 0.005 au; red = negative) for the HOMO→LUMO excitations of two hydrogen-bonded OLH– H_2O complexes. Obtained from LR-TDDFT calculations with PBE0 functional and 6-31G(d) basis set.

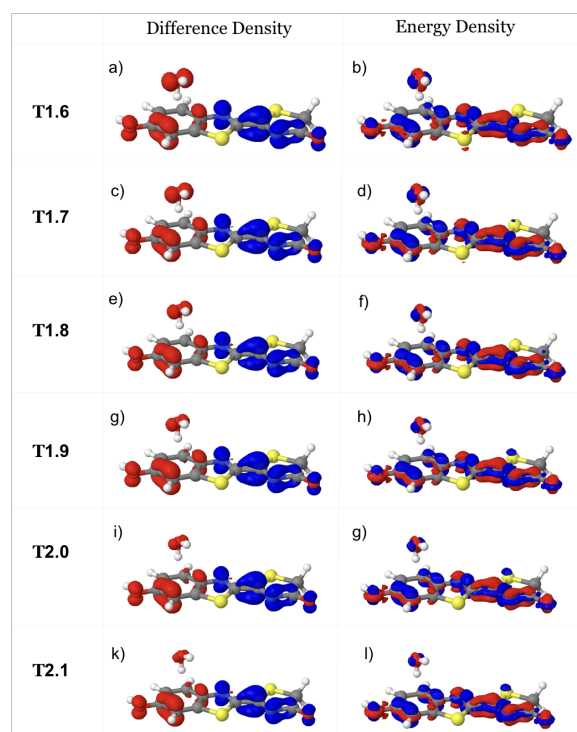


Fig. 6 Difference density and excitation energy density plots (isovalue surface of 0.005 au; red = negative) for the HOMO→LUMO excitations of six T-shape OLH– H_2O complexes (with the distance between water hydrogen and OLH benzene ring center ranging from 1.6 to 2.1 Å). Obtained from LR-TDDFT calculations with PBE0 functional and 6-31G(d) basis set.

The HOMO→LUMO vertical excitation of oxyluciferin involves a partial charge transfer from the benzothiazole ring to the thiazole ring. As shown in the difference density plots in Figure 5a and 5c, such a partial charge transfer was largely unchanged upon the binding of a water molecule in the two hydrogen bond complexes. In Table 2, the fragment charges on OLH or water in **HB1** and **HB2** were found to be only $0.006 e^-$. Accordingly, the excitation energy densities in Figure 5b and 5d remained localized on OLH, with the fragment excitation energies integrated to only 0.02 eV (**HB1**) and -0.01 eV (**HB2**) on H_2O molecule in Table 2.

Table 2 Binding energies, excitation character metrics (Λ and S_{DA}), FBH fragment charges, and FBH fragment excitation energies for HOMO→LUMO excitations of three neutral OLH–H₂O configurations. Obtained from LR-TDDFT calculations with the PBE0 functional and 6-31G(d) basis set.

Con	ΔE_{bind} (kcal/mol)		ES#	Λ	S_{DA}	ΔQ_A (au)		ω_A or ω (eV)		
	w/o BSSE	w/ BSSE				OLH	H ₂ O	OLH	H ₂ O	Total
HB1	−8.798	−6.599	1	0.627	0.632	0.006	−0.006	3.495	0.020	3.515
HB2	−6.115	−4.092	2	0.640	0.632	−0.006	0.006	3.638	−0.010	3.628
T1.6	7.224	7.888	1	0.594	0.607	−0.150	0.150	2.396	1.108	3.504
T1.7	4.192	7.554	1	0.602	0.616	−0.118	0.118	2.719	0.828	3.547
T1.8	1.954	4.910	1	0.602	0.636	−0.087	0.087	2.994	0.582	3.576
T1.9	0.380	2.934	2	0.615	0.631	−0.067	0.067	3.175	0.420	3.595
T2.0	−0.660	1.550	2	0.622	0.629	−0.052	0.052	3.305	0.303	3.608
T2.1	−1.361	0.502	2	0.625	0.630	−0.037	0.037	3.412	0.197	3.609

However, the picture can be quite different when oxyluciferin formed a T-shape complex (T) with a water molecule. As shown in the left column of Figure 6, the detachment density could more easily “spill” over to the water molecule, which corresponds to an extension of OLH HOMO to the water molecule. For the HOMO→LUMO excitation of these T-shape complexes, Table 2 thus showed a net loss of 0.037 to 0.150 e^- from the water molecule. This was accompanied by a “spillover” of the excitation energy density to the water molecule in each of these T-shape complexes (see the right column of Figure 6), with the fragment excitation energy on water computed to be 0.197 to 1.108 eV.

5 Discussions

Functional and Basis Set. So far, we have focused our report on LR-TDDFT calculations using the PBE0 functional and 6-31G(d) basis set. Such a choice was made on two practical considerations — the easiness of identifying the charge-transfer excited state and a moderate computational cost. But, As shown in Tables S1–S9, our energy density analysis is also fully functioning with larger Pople basis sets,^{85,93} such as 6-31+G(d), 6-311G(d), 6-311++G(d,p), or Dunning correlation-consistent basis sets,^{94,95} such as cc-pVDZ, aug-cc-pVDZ, cc-pVTZ and aug-cc-pVTZ.

Our implementation of excitation energy densities is also applicable to other functionals, such as pure and range-separated functionals, which require the use of appropriate electron repulsion operators, if any, in the calculation of exchange energy density components. Results with the PBE⁹⁶ and ω B97X-D functionals are shown in Tables S1, S3, S4, S6, S7, and S9 for C₂H₄–C₂F₄ dimers. For local excitations, the excitation energy remain localized with these two functionals. On the other hand, in a charge-transfer excitation, the acceptor portion of the excitation energy (which can be interpreted as the effective energy of the “particle”) arises from a cancellation of the kinetic energy of the “particle” and other contributions. While it is consistently positive with the ω B97X-D functional, it can acquire a negative value with PBE and PBE0 functionals, likely due to lower (and sometimes even negative) LUMO energy values.

Computational Cost. Within our preliminary implementation, the computational cost for obtaining excitation energy density

arises mainly from the evaluation of $V_{\lambda\sigma}$, which is the grid-based electrostatic potential of each function pair (*i.e.* pairs of atomic basis functions) in Eq. 14. $V_{\lambda\sigma}$ is needed in the construction of Coulomb and exchange energy densities in Eqs. 26 and 27. Such a calculation would become rather prohibitive for large systems and/or larger basis sets, but it can be greatly accelerated by the use of the pseudospectral method⁹⁷ as shown by Nakai and coworkers.⁹⁸ On the other hand, the resolution-of-the-identity (RI) approach^{99–106} was employed in the past to approximate the ground-state Hartree-Fock exchange energy density,^{107,108} and thus we anticipate a similar use of the RI approach to accelerate the evaluation of excitation energy densities.

Table 3 TDDFT (for the full system), TDDFT/TIP3P excitation energies, and the differences between them (in eV) for the HOMO→LUMO excitations of the HB1, HB2, and T-shape configurations of neutral OLH–H₂O calculated with the PBE0 functional and 6-31G(d) basis set by Q-CHEM.

Configuration	ES#	$\omega_{\text{Full-TDDFT}}$	$\omega_{\text{TDDFT/TIP3P}}$	$\Delta\omega$
HB1	1	3.516	3.545	0.039
HB2	2	3.630	3.620	−0.010
T1.6	1	3.507	3.663	0.156
T1.7	1	3.550	3.663	0.113
T1.8	1	3.578	3.661	0.073
T1.9	2	3.597	3.656	0.059
T2.0	2	3.610	3.654	0.044
T2.1	2	3.611	3.642	0.031

Fluorophore-Solvent Charge Transfer. For the T-shape oxyluciferin-water complexes, we have noticed a “spillover” of detachment/attachment density and excitation energy density to the water molecule. This is ultimately due to a strong interaction between the fluorophore and water frontier orbitals, which can only be captured by coupling orbitals from different fragments.¹⁰⁹ As shown in Table 3, this has led the LR-TDDFT/TIP3P model to systematically overestimate the vertical excitation energies of T-shape complexes.

An individual T-shape complex can be energetically unfavorable, as evident by the binding energies in Table 2. In TDDFT/TIP3P

molecular dynamics simulation of the solvated OLH (and several other fluorophores), we have nevertheless observed multiple water molecules (in the first solvation shell) forming T-shape complexes with the fluorophore. Lacking a treatment of charge-transfer interactions between the QM and MM regions, LR-TDDFT/TIP3P can systematically overestimate the vertical excitation energy of the fluorophore (within in first solvation shell) by as much as 0.10–0.15 eV. For a more accurate description of solvatochromic effect (especially with multiple solvents), it is therefore desirable to extend orbital-dependent inter-fragment charge-transfer models (such as the EFP model)¹¹⁰ to excited state calculations.

6 Conclusions

In this article, we presented a method for distributing the LR-TDDFT excitation energy over the real space, and thus for acquiring the grid-based excitation energy density for each excited state. Due to the kinetic energy density term, the excitation energy distribution was found to be slightly more complicated than the difference electron density (between the ground and excited states).

For locally-excited states (as indicated by the attachment/detachment densities and changes in fragment charges), the excitation energy density was concentrated on a single molecular fragment, just as expected. In charge-transfer excitations, such as the ones in the C₂H₄–C₂F₄ complex, the excitation energy density would be distributed over both donor and acceptor fragments, with a higher percentage of the excitation energy allocated on the donor fragment. Fragment excitation energies from a charge-transfer excitation can be regarded as the effective energies for the “hole” and “particle”, respectively.

For excitations with a partial charge transfer between a fluorophore and water, such as T-shape OLH–water complexes, a small percentage of the excitation energy was found on the water molecules. The challenge to model such an effect with QM/MM-type methods stems from inter-fragment orbital mixing and might motivate the development of new methodologies to capture solute-solvent charge-transfer effects on electronic transitions.

Conflicts of interest

There are no conflicts to declare.

Acknowledgements

YS thanks Drs. John Herbert, Aurelian de la Lande, Xiaosong Li, Felix Plasser, and Weitao Yang for helpful discussions. We thank the reviewers for their insightful comments and helpful suggestions. YS is supported by the National Institutes of Health (grant: R01GM135392), Oklahoma Center for the Advancement of Science and Technology (grant: HR18-130), and the Office of the Vice President of Research and the College of Art and Sciences at the University of Oklahoma (OU). WL acknowledges financial support from the National Natural Science Foundation of China (Grant Nos. 21573177 and 21833006). BW acknowledges funding from the US Department of Energy (Grant No. DE-SC0020300). CMA is supported by the Department of Energy under grant DE-SC0012273. The computing for this project was performed at the OU Supercomputing Center for Education & Research (OSCER)

and the Center of Functional Nanomaterials (CFN). CFN is a U.S. DOE Office of Science Facility, at the Brookhaven National Laboratory under Contract No. DE-SC0012704.

References

- 1 J. W. Storer, D. J. Giesen, C. J. Cramer and D. G. Truhlar, Class IV Charge Models: A New Semiempirical Approach in Quantum Chemistry, *J. Comput. Aid. Mol. Des.*, 1995, **9**, 87–110.
- 2 A. M. Pendas, M. A. Blanco and E. Francisco, Chemical Fragments in Real Space: Definitions, Properties, and Energetic Decompositions, *J. Comput. Chem.*, 2007, **28**, 161–184.
- 3 Y. Mei, A. C. Simmonett, F. C. Pickard, R. A. DiStasio, B. R. Brooks and Y. Shao, Numerical Study on the Partitioning of the Molecular Polarizability into Fluctuating Charge and Induced Atomic Dipole Contributions, *J. Phys. Chem. A*, 2015, **119**, 5865–5882.
- 4 R. S. Mulliken, Electronic Population Analysis on LCAO–MO Molecular Wave Functions. I, *J. Chem. Phys.*, 1955, **23**, 1833–1840.
- 5 P.-O. Löwdin, On the Non-Orthogonality Problem Connected with the Use of Atomic Wave Functions in the Theory of Molecules and Crystals, *J. Chem. Phys.*, 1950, **18**, 365–375.
- 6 J. Baker, Classical Chemical Concepts from ab initio SCF Calculations, *Theor. Chim. Acta*, 1985, **68**, 221–229.
- 7 R. F. W. Bader and P. M. Beddall, Virial Field Relationship for Molecular Charge Distributions and the Spatial Partitioning of Molecular Properties, *J. Chem. Phys.*, 1972, **56**, 3320–3329.
- 8 R. F. W. Bader, *Atoms in Molecules: A Quantum Theory*, Clarendon Press ; Oxford University Press, Oxford [England] : New York, 1994.
- 9 R. F. W. Bader and C. F. Matta, Atomic Charges Are Measurable Quantum Expectation Values: A Rebuttal of Criticisms of QTAIM Charges, *J. Phys. Chem. A*, 2004, **108**, 8385–8394.
- 10 J. P. Foster and F. Weinhold, Natural hybrid orbitals, *J. Am. Chem. Soc.*, 1980, **102**, 7211–7218.
- 11 A. E. Reed, R. B. Weinstock and F. Weinhold, Natural Population Analysis, *J. Chem. Phys.*, 1985, **83**, 735–746.
- 12 E. D. Glendening, C. R. Landis and F. Weinhold, Natural Bond Orbital Methods, *WIREs Comput. Mol. Sci.*, 2012, **2**, 1–42.
- 13 U. C. Singh and P. A. Kollman, An approach to computing electrostatic charges for molecules, *J. Comput. Chem.*, 1984, **5**, 129–145.
- 14 L. E. Chirlian and M. M. Francl, Atomic Charges Derived from Electrostatic Potentials: A Detailed Study, *J. Comput. Chem.*, 1987, **8**, 894–905.
- 15 C. M. Breneman and K. B. Wiberg, Determining Atom-Centered Monopoles from Molecular Electrostatic Potentials. The Need for High Sampling Density in Formamide Conformational Analysis, *J. Comput. Chem.*, 1990, **11**, 361–373.
- 16 B. H. Besler, K. M. Merz and P. A. Kollman, Atomic Charges Derived from Semiempirical Methods, *J. Comput. Chem.*, 1990, **11**, 431–439.
- 17 C. I. Bayly, P. Cieplak, W. Cornell and P. A. Kollman, A well-

- behaved electrostatic potential based method using charge restraints for deriving atomic charges: the RESP model, *J. Phys. Chem.*, 1993, **97**, 10269–10280.
- 18 W. D. Cornell, P. Cieplak, C. I. Bayly and P. A. Kollman, Application of RESP Charges to Calculate Conformational Energies, Hydrogen Bond Energies, and Free Energies of Solvation, *J. Am. Chem. Soc.*, 1993, **115**, 9620–9631.
- 19 M. M. Francl, C. Carey, L. E. Chirlian and D. M. Gange, Charges Fit to Electrostatic Potentials. II. Can Atomic Charges Be Unambiguously Fit to Electrostatic Potentials?, *J. Comput. Chem.*, 1996, **17**, 367–383.
- 20 A. Laio, J. VandeVondele and U. Rothlisberger, D-RESP: Dynamically Generated Electrostatic Potential Derived Charges from Quantum Mechanics/Molecular Mechanics Simulations, *J. Phys. Chem. B*, 2002, **106**, 7300–7307.
- 21 H. Hu, Z. Lu and W. Yang, Fitting Molecular Electrostatic Potentials from Quantum Mechanical Calculations, *J. Chem. Theory Comput.*, 2007, **3**, 1004–1013.
- 22 M. Schauerl, P. S. Nerenberg, H. Jang, L.-P. Wang, C. I. Bayly, D. L. Mobley and M. K. Gilson, Non-Bonded Force Field Model with Advanced Restrained Electrostatic Potential Charges (RESP2), *Commun. Chem.*, 2020, **3**, 44.
- 23 A. D. Becke, A multicenter numerical integration scheme for polyatomic molecules, *J. Chem. Phys.*, 1988, **88**, 2547–2553.
- 24 F. L. Hirshfeld, Bonded-atom fragments for describing molecular charge densities, *Theor. Chim. Acta*, 1977, **44**, 129–138.
- 25 F. L. Hirshfeld, XVII. Spatial Partitioning of Charge Density, *Israel J. Chem.*, 1977, **16**, 198–201.
- 26 F. De Proft, C. Van Alsenoy, A. Peeters, W. Langenaeker and P. Geerlings, Atomic Charges, Dipole moments, and Fukui Functions Using the Hirshfeld Partitioning of the Electron Density, *J. Comput. Chem.*, 2002, **23**, 1198–1209.
- 27 J. Rezac and A. de la Lande, Robust, Basis-Set Independent Method for the Evaluation of Charge-Transfer Energy in Non-covalent Complexes, *J. Chem. Theory Comput.*, 2015, **11**, 528–537.
- 28 P. Bultinck, C. V. Alsenoy, P. W. Ayers and R. Carbó-Dorca, Critical analysis and extension of the Hirshfeld atoms in molecules, *J. Chem. Phys.*, 2007, **126**, 144111.
- 29 P. Bultinck, P. W. Ayers, S. Fias, K. Tiels and C. Van Alsenoy, Uniqueness and Basis Set Dependence of Iterative Hirshfeld Charges, *Chem. Phys. Lett.*, 2007, **444**, 205–208.
- 30 P. Bultinck, D. L. Cooper and D. Van Neck, Comparison of the Hirshfeld-I and Iterated Stockholder Atoms in Molecules Schemes, *Phys. Chem. Chem. Phys.*, 2009, **11**, 3424.
- 31 D. M. Elking, L. Perera and L. G. Pedersen, HPAM: Hirshfeld Partitioned Atomic Multipoles, *Comput. Phys. Commun.*, 2012, **183**, 390–397.
- 32 T. C. Lillestolen and R. J. Wheatley, Redefining the Atom: Atomic Charge Densities Produced by an Iterative Stockholder Approach, *Chem. Commun.*, 2008, 5909.
- 33 T. Verstraelen, P. Ayers, V. Van Speybroeck and M. Waroquier, The Conformational Sensitivity of Iterative Stockholder Partitioning Schemes, *Chem. Phys. Lett.*, 2012, **545**, 138–143.
- 34 T. Verstraelen, P. W. Ayers, V. Van Speybroeck and M. Waroquier, Hirshfeld-E Partitioning: AIM Charges with an Improved Trade-off between Robustness and Accurate Electrostatics, *J. Chem. Theory Comput.*, 2013, **9**, 2221–2225.
- 35 T. A. Manz and D. S. Sholl, Chemically Meaningful Atomic Charges That Reproduce the Electrostatic Potential in Periodic and Nonperiodic Materials, *J. Chem. Theory Comput.*, 2010, **6**, 2455–2468.
- 36 T. A. Manz and D. S. Sholl, Improved Atoms-in-Molecule Charge Partitioning Functional for Simultaneously Reproducing the Electrostatic Potential and Chemical States in Periodic and Nonperiodic Materials, *J. Chem. Theory Comput.*, 2012, **8**, 2844–2867.
- 37 T. A. Manz and N. G. Limas, Introducing DDEC6 Atomic Population Analysis: Part 1. Charge Partitioning Theory and Methodology, *RSC Adv.*, 2016, **6**, 47771–47801.
- 38 N. G. Limas and T. A. Manz, Introducing DDEC6 Atomic Population Analysis: Part 2. Computed Results for a Wide Range of Periodic and Nonperiodic Materials, *RSC Adv.*, 2016, **6**, 45727–45747.
- 39 T. A. Manz, Introducing DDEC6 Atomic Population Analysis: Part 3. Comprehensive Method to Compute Bond Orders, *RSC Adv.*, 2017, **7**, 45552–45581.
- 40 R. M. Olson, A. V. Marenich, C. J. Cramer and D. G. Truhlar, Charge Model 4 and Intramolecular Charge Polarization, *J. Chem. Theory Comput.*, 2007, **3**, 2046–2054.
- 41 A. V. Marenich, S. V. Jerome, C. J. Cramer and D. G. Truhlar, Charge Model 5: An Extension of Hirshfeld Population Analysis for the Accurate Description of Molecular Interactions in Gaseous and Condensed Phases, *J. Chem. Theory Comput.*, 2012, **8**, 527–541.
- 42 R. G. Parr and W. Yang, Density Functional Approach to the Frontier-Electron Theory of Chemical Reactivity, *J. Am. Chem. Soc.*, 1984, **106**, 4049–4050.
- 43 W. Yang, A. J. Cohen, F. De Proft and P. Geerlings, Analytical Evaluation of Fukui Functions and Real-Space Linear Response Function, *J. Chem. Phys.*, 2012, **136**, 144110.
- 44 F. Heidar-Zadeh, R. A. Miranda-Quintana, T. Verstraelen, P. Bultinck and P. W. Ayers, When is the Fukui Function Not Normalized? The Danger of Inconsistent Energy Interpolation Models in Density Functional Theory, *J. Chem. Theory Comput.*, 2016, **12**, 5777–5787.
- 45 F. Plasser, M. Wormit and A. Dreuw, New tools for the systematic analysis and visualization of electronic excitations. I. Formalism, *J. Chem. Phys.*, 2014, **141**, 024106.
- 46 F. Plasser, S. A. Bäßler, M. Wormit and A. Dreuw, New tools for the systematic analysis and visualization of electronic excitations. II. Applications, *J. Chem. Phys.*, 2014, **141**, 024107.
- 47 F. Plasser, TheoDORE: A toolbox for a Detailed and Automated Analysis of Electronic Excited State Computations, *J. Chem. Phys.*, 2020, **152**, 084108.
- 48 A. I. Krylov, From Orbitals to Observables and Back, *J. Chem. Phys.*, 2020, **153**, 080901.
- 49 T. Le Bahers, C. Adamo and I. Ciofini, A Qualitative Index of Spatial Extent in Charge-Transfer Excitations, *J. Chem. Theory*

- Comput.*, 2011, **7**, 2498–2506.
- 50 C. A. Guido, P. Cortona, B. Mennucci and C. Adamo, On the Metric of Charge Transfer Molecular Excitations: A Simple Chemical Descriptor, *J. Chem. Theory Comput.*, 2013, **9**, 3118–3126.
- 51 T. Etienne, X. Assfeld and A. Monari, Toward a Quantitative Assessment of Electronic Transitions' Charge-Transfer Character, *J. Chem. Theory Comput.*, 2014, **10**, 3896–3905.
- 52 T. Etienne, X. Assfeld and A. Monari, New Insight into the Topology of Excited States through Detachment/Attachment Density Matrices-Based Centroids of Charge, *J. Chem. Theory Comput.*, 2014, **10**, 3906–3914.
- 53 T. Etienne, Probing the Locality of Excited States with Linear Algebra, *J. Chem. Theory Comput.*, 2015, **11**, 1692–1699.
- 54 B. Moore, H. Sun, N. Govind, K. Kowalski and J. Autschbach, Charge-Transfer Versus Charge-Transfer-Like Excitations Revisited, *J. Chem. Theory Comput.*, 2015, **11**, 3305–3320.
- 55 G. Bistoni, L. Belpassi and F. Tarantelli, Advances in Charge Displacement Analysis, *J. Chem. Theory Comput.*, 2016, **12**, 1236–1244.
- 56 M. Savarese, C. A. Guido, E. Bremond, I. Ciofini and C. Adamo, Metrics for Molecular Electronic Excitations: A Comparison between Orbital- and Density-Based Descriptors, *J. Phys. Chem. A*, 2017, **121**, 7543–7549.
- 57 M. Campetella, F. Maschietto, M. J. Frisch, G. Scalmani, I. Ciofini and C. Adamo, Charge Transfer Excitations in TDDFT: A Ghost-Hunter Index, *J. Comput. Chem.*, 2017, **38**, 2151–2156.
- 58 M. Alipour and S. Damiri, Development of a Novel Index for Analysis of Electronically Excited States, *ChemPhysChem*, 2017, **18**, 480–487.
- 59 M. J. G. Peach, P. Benfield, T. Helgaker and D. J. Tozer, Excitation energies in density functional theory: An evaluation and a diagnostic test, *J. Chem. Phys.*, 2008, **128**, 044118.
- 60 S. A. Mewes, F. Plasser, A. Krylov and A. Dreuw, Benchmarking Excited-State Calculations Using Exciton Properties, *Journal of Chemical Theory and Computation*, 2018, **14**, 710–725.
- 61 M. Hoffmann, S. A. Mewes, S. Wieland, C. Popp and A. Dreuw, Electron–Hole Correlation as Unambiguous and Universal Classification for the Nature of Low-Lying $\pi\pi^*$ States of Nitrogen Heterocycles, *J. Phys. Chem. Lett.*, 2019, **10**, 6112–6117.
- 62 S. A. Mewes and A. Dreuw, Density-based descriptors and exciton analyses for visualizing and understanding the electronic structure of excited states, *Phys. Chem. Chem. Phys.*, 2019, **21**, 2843–2856.
- 63 P. Kimber and F. Plasser, Toward an Understanding of Electronic Excitation Energies Beyond the Molecular Orbital Picture, *Phys. Chem. Chem. Phys.*, 2020, **22**, 6058–6080.
- 64 M. Head-Gordon, A. M. Grana, D. Maurice and C. A. White, Analysis of Electronic Transitions as the Difference of Electron Attachment and Detachment Densities, *J. Phys. Chem.*, 1995, **99**, 14261–14270.
- 65 H. Nakai, Energy density analysis with Kohn–Sham orbitals, *Chemical Physics Letters*, 2002, **363**, 73–79.
- 66 Y. Imamura, A. Takahashi and H. Nakai, Grid-based energy density analysis: Implementation and assessment, *J. Chem. Phys.*, 2007, **126**, 034103.
- 67 H. Nakai, H. Ohashi, Y. Imamura and Y. Kikuchi, Bond energy analysis revisited and designed toward a rigorous methodology, *J. Chem. Phys.*, 2011, **135**, 124105.
- 68 Y. Imamura and H. Nakai, Energy Density Analysis for Second-Order Moller-Plesset perturbation Theory and Coupled-Cluster Theory with Singles and Doubles: Application to $C_2H_4-CH_4$ Complexes, *J. Comput. Chem.*, 2008, **29**, 1555–1563.
- 69 M. E. Casida, in *Recent Advances in Density Functional Methods Part I.*, World Scientific, 1995, p. 155.
- 70 R. Bauernschmitt and R. Ahlrichs, Treatment of Electronic Excitations within the Adiabatic Approximation of Time Dependent Density Functional Theory, *Chem. Phys. Lett.*, 1996, **256**, 454–464.
- 71 S. Hirata and M. Head-Gordon, Time-Dependent Density Functional Theory for Radicals, *Chem. Phys. Lett.*, 1999, **302**, 375–382.
- 72 A. Dreuw and M. Head-Gordon, Single-Reference ab Initio Methods for the Calculation of Excited States of Large Molecules, *Chem. Rev.*, 2005, **105**, 4009–4037.
- 73 M. Casida and M. Huix-Rotllant, Progress in Time-Dependent Density-Functional Theory, *Ann. Rev. Phys. Chem.*, 2012, **63**, 287–323.
- 74 J. Yang, Z. Pei, J. Deng, Y. Mao, Q. Wu, Z. Yang, B. Wang, C. M. Aikens, W. Liang and Y. Shao, Analysis and Visualization of Energy Densities. I. Insights from Real-Time Time-Dependent Density Functional Theory Simulations, *Under Review*.
- 75 J. Tao, J. P. Perdew, V. N. Staroverov and G. E. Scuseria, Climbing the Density Functional Ladder: Nonempirical Meta-Generalized Gradient Approximation Designed for Molecules and Solids, *Phys. Rev. Lett.*, 2003, **91**, 146401.
- 76 Y. Zhao and D. G. Truhlar, The M06 Suite of Density Functionals for Main Group Thermochemistry, Thermochemical Kinetics, Noncovalent Interactions, Excited states, and Transition Elements: Two New Functionals and Systematic Testing of Four M06-Class Functionals and 12 Other Functionals, *Theor. Chem. Acc.*, 2008, **120**, 215–241.
- 77 D. Maurice and M. Head-Gordon, Analytical Second Derivatives for Excited Electronic States Using the Single Excitation Configuration Interaction Method: Theory and Application to Benzo[a]pyrene and Chalcone, *Mol. Phys.*, 1999, **96**, 1533–1541.
- 78 F. Liu, Z. Gan, Y. Shao, C.-P. Hsu, A. Dreuw, M. Head-Gordon, B. T. Miller, B. R. Brooks, J.-G. Yu, T. R. Furlani and J. Kong, A Parallel Implementation of the Analytic Nuclear Gradient for Time-Dependent Density Functional Theory within the Tamm-Dancoff Approximation, *Mol. Phys.*, 2010, **108**, 2791–2800.
- 79 N. Holmberg and K. Laasonen, Efficient Constrained Density Functional Theory Implementation for Simulation of Condensed Phase Electron Transfer Reactions, *J. Chem. Theory Comput.*, 2017, **13**, 587–601.

- 80 Y. Mao, Q. Ge, P. R. Horn and M. Head-Gordon, On the Computational Characterization of Charge-Transfer Effects in Noncovalently Bound Molecular Complexes, *J. Chem. Theory Comput.*, 2018, **14**, 2401–2417.
- 81 Y. Shao, Y. Mei, D. Sundholm and V. R. I. Kaila, Benchmarking the Performance of Time-Dependent Density Functional Theory Methods on Biochromophores, *J. Chem. Theory Comput.*, 2020, **16**, 587–600.
- 82 A. Dreuw, J. L. Weisman and M. Head-Gordon, Long-range charge-transfer excited states in time-dependent density functional theory require non-local exchange, *J. Chem. Phys.*, 2003, **119**, 2943–2946.
- 83 M. A. Rohrdanz, K. M. Martins and J. M. Herbert, A long-range-corrected density functional that performs well for both ground-state properties and time-dependent density functional theory excitation energies, including charge-transfer excited states, *J. Chem. Phys.*, 2009, **130**, 054112.
- 84 J.-D. Chai and M. Head-Gordon, Long-Range Corrected Hybrid Density Functionals with Damped Atom-Atom Dispersion Corrections, *Phys. Chem. Chem. Phys.*, 2008, **10**, 6615.
- 85 R. Krishnan, J. S. Binkley, R. Seeger and J. A. Pople, Self-Consistent Molecular Orbital Methods. XX. A Basis Set for Correlated Wave Functions, *J. Chem. Phys.*, 1980, **72**, 650–654.
- 86 Y.-Y. Cheng and Y.-J. Liu, What Exactly Is the Light Emitter of a Firefly?, *J. Chem. Theory Comput.*, 2015, **11**, 5360–5370.
- 87 Q. Sun, T. C. Berkelbach, N. S. Blunt, G. H. Booth, S. Guo, Z. Li, J. Liu, J. D. McClain, E. R. Sayfutyarova, S. Sharma, S. Wouters and G. K. Chan, PySCF: the Python-Based Simulations of Chemistry Framework, *WIREs Comput. Mol. Sci.*, 2018, **8**, e1340.
- 88 Y. Shao, Z. Gan, E. Epifanovsky, A. T. Gilbert, M. Wormit, J. Kussmann, A. W. Lange, A. Behn, J. Deng, X. Feng, D. Ghosh, M. Goldey, P. R. Horn, L. D. Jacobson, I. Kaliman, R. Z. Khaliullin, T. Kusnerik, A. Landau, J. Liu, E. I. Proynov, Y. M. Rhee, R. M. Richard, M. A. Rohrdanz, R. P. Steele, E. J. Sundstrom, H. L. Woodcock, P. M. Zimmerman, D. Zuev, B. Albrecht, E. Alguire, B. Austin, G. J. O. Beran, Y. A. Bernard, E. Berquist, K. Brandhorst, K. B. Bravaya, S. T. Brown, D. Casanova, C.-M. Chang, Y. Chen, S. H. Chien, K. D. Closser, D. L. Crittenden, M. Diedenhofen, R. A. DiStasio, H. Do, A. D. Dutoi, R. G. Edgar, S. Fatehi, L. Fusti-Molnar, A. Ghysels, A. Golubeva-Zadorozhnaya, J. Gomes, M. W. Hanson-Heine, P. H. Harbach, A. W. Hauser, E. G. Hohenstein, Z. C. Holden, T.-C. Jagau, H. Ji, B. Kaduk, K. Khistyayev, J. Kim, J. Kim, R. A. King, P. Klunzinger, D. Kosenkov, T. Kowalczyk, C. M. Krauter, K. U. Lao, A. D. Laurent, K. V. Lawler, S. V. Levchenko, C. Y. Lin, F. Liu, E. Livshits, R. C. Lochan, A. Luenser, P. Manohar, S. F. Manzer, S.-P. Mao, N. Mardirossian, A. V. Marenich, S. A. Maurer, N. J. Mayhall, E. Neuscamman, C. M. Oana, R. Olivares-Amaya, D. P. O'Neill, J. A. Parkhill, T. M. Perrine, R. Peverati, A. Prociuk, D. R. Rehn, E. Rosta, N. J. Russ, S. M. Sharada, S. Sharma, D. W. Small, A. Sodt, T. Stein, D. Stuck, Y.-C. Su, A. J. Thom, T. Tsuchimochi, V. Vanovschi, L. Vogt, O. Vydrov, T. Wang, M. A. Watson, J. Wenzel, A. White, C. F. Williams, J. Yang, S. Yeganeh, S. R. Yost, Z.-Q. You, I. Y. Zhang, X. Zhang, Y. Zhao, B. R. Brooks, G. K. Chan, D. M. Chipman, C. J. Cramer, W. A. Goddard, M. S. Gordon, W. J. Hehre, A. Klamt, H. F. Schaefer, M. W. Schmidt, C. D. Sherrill, D. G. Truhlar, A. Warshel, X. Xu, A. Aspuru-Guzik, R. Baer, A. T. Bell, N. A. Besley, J.-D. Chai, A. Dreuw, B. D. Dunietz, T. R. Furlani, S. R. Gwaltney, C.-P. Hsu, Y. Jung, J. Kong, D. S. Lambrecht, W. Liang, C. Ochsenfeld, V. A. Rassolov, L. V. Slipchenko, J. E. Subotnik, T. Van Voorhis, J. M. Herbert, A. I. Krylov, P. M. Gill and M. Head-Gordon, Advances in Molecular Quantum Chemistry Contained in the Q-Chem 4 Program Package, *Mol. Phys.*, 2015, **113**, 184–215.
- 89 C. Adamo and V. Barone, Toward Reliable Density Functional Methods Without Adjustable Parameters: The PBE0 Model, *J. Chem. Phys.*, 1999, **110**, 6158–6170.
- 90 W. J. Hehre, R. Ditchfield and J. A. Pople, Self-Consistent Molecular Orbital Methods. XII. Further Extensions of Gaussian-Type Basis Sets for Use in Molecular Orbital Studies of Organic Molecules, *J. Chem. Phys.*, 1972, **56**, 2257–2261.
- 91 P. C. Hariharan and J. A. Pople, The influence of polarization functions on molecular orbital hydrogenation energies, *Theor. Chim. Acta*, 1973, **28**, 213–222.
- 92 R. L. Martin, Natural Transition Orbitals, *J. Chem. Phys.*, 2003, **118**, 4775–4777.
- 93 T. Clark, J. Chandrasekhar, G. W. Spitznagel and P. V. R. Schleyer, Efficient Diffuse Function-augmented Basis Sets for Anion Calculations. III. The 3-21+G Basis Set for First-row Elements, Li-F, *J. Chem. Phys.*, 1983, **4**, 294–301.
- 94 T. H. Dunning, Gaussian Basis Sets for Use in Correlated Molecular Calculations. I. The Atoms Boron Through Neon and Hydrogen, *J. Chem. Phys.*, 1989, **90**, 1007–1023.
- 95 R. A. Kendall, T. H. Dunning and R. J. Harrison, Electron Affinities of the First-Row Atoms Revisited. Systematic Basis Sets and Wave Functions, *J. Chem. Phys.*, 1992, **96**, 6796–6806.
- 96 J. P. Perdew, K. Burke and M. Ernzerhof, Generalized Gradient Approximation Made Simple, *Phys. Rev. Lett.*, 1996, **77**, 3865–3868.
- 97 R. A. Friesner, Solution of Self-Consistent Field Electronic Structure Equations by a Pseudospectral Method, *Chem. Phys. Lett.*, 1985, **116**, 39–43.
- 98 Y. Imamura, A. Takahashi and H. Nakai, Grid-Based Energy Density Analysis: Implementation and Assessment, *J. Chem. Phys.*, 2007, **126**, 034103.
- 99 O. Vahtras, J. Almlöf and M. Feyereisen, Integral Approximations for LCAO-SCF Calculations, *Chem. Phys. Lett.*, 1993, **213**, 514–518.
- 100 K. Eichkorn, O. Treutler, H. Ohm, M. Haser and R. Ahlrichs, Auxiliary Basis Sets to Approximate Coulomb Potentials, *Chem. Phys. Lett.*, 1995, **240**, 283–290.
- 101 K. Eichkorn, F. Weigend, O. Treutler and R. Ahlrichs, Auxiliary Basis Sets for Main Row Atoms and Transition Metals and Their Use to Approximate Coulomb Potentials, *Theor. Chem. Acta*, 1997, **97**, 119–124.
- 102 B. Dunlap, Robust Variational Fitting: Gaspar's Variational

- Exchange Can Accurately Be Treated Analytically, *J. Mol. Struct. THEOCHEM*, 2000, **501-502**, 221–228.
- 103 B. Dunlap, Robust and Variational Fitting: Removing the Four-Center Integrals from Center Stage in Quantum Chemistry, *J. Mol. Struct. THEOCHEM*, 2000, **529**, 37–40.
- 104 Y. Jung, A. Sodt, P. M. W. Gill and M. Head-Gordon, Auxiliary Basis Expansions for Large-Scale Electronic Structure Calculations, *Proc. Natl. Acad. Sci. USA*, 2005, **102**, 6692–6697.
- 105 D. S. Hollman, H. F. Schaefer and E. F. Valeev, Semi-Exact Concentric Atomic Density Fitting: Reduced Cost and Increased Accuracy Compared to Standard Density Fitting, *J. Chem. Phys.*, 2014, **140**, 064109.
- 106 H. F. Schurkus, A. Luenser and C. Ochsenfeld, Almost Error-Free Resolution-of-the-Identity Correlation Methods by Null Space Removal of the Particle-Hole Interactions, *J. Chem. Phys.*, 2017, **146**, 211106.
- 107 E. Proynov, Y. Shao and J. Kong, Efficient Self-Consistent DFT Calculation of Nondynamic Correlation Based on the B05 Method, *Chem. Phys. Lett.*, 2010, **493**, 381–385.
- 108 E. Proynov, F. Liu, Y. Shao and J. Kong, Improved Self-Consistent and Resolution-of-Identity Approximated Becke'05 Density Functional Model of Nondynamic Electron Correlation, *J. Chem. Phys.*, 2012, **136**, 034102.
- 109 Y. Mao, M. Head-Gordon and Y. Shao, Unraveling Substituent Effects on Frontier Orbitals of Conjugated Molecules Using an Absolutely Localized Molecular Orbital Based Analysis, *Chem. Sci.*, 2018, **9**, 8598–8607.
- 110 M. S. Gordon, D. G. Fedorov, S. R. Pruitt and L. V. Slipchenko, Fragmentation Methods: A Route to Accurate Calculations on Large Systems, *Chem. Rev.*, 2012, **112**, 632–672.

